Invariant-mass spectroscopy of math xmlns="http://www.w3.org/1998/Math/MathML">mmultiscripts>mi mathvariant="normal">B/mi> mprescripts>/mprescripts>none>/none>mn>10/mn>/mmultiscripts>mo>,/mo>mo> /mo>mmultiscripts>mi mathvariant="normal">C/mi>mprescripts>/mprescripts>none>/none>mn>11/mn>/mmultiscripts>mo>,/mo>mo> /mo>mmultiscripts>mi mathvariant="normal">F/mi>mprescripts>/mprescripts>none>/none>mn>14/mn>/mmultiscripts>mo>,/mo>mo> /mo>mmultiscripts>mi mathvariant="normal">F/mi>mprescripts>/mprescripts>none>/none>mn>16/mn>/mmultiscripts>/math>, and math xmlns="http://www.w3.org/1998/Math/MathML">mmultiscripts>mi>Na/mi>mprescripts>/mprescripts>none>/none>mn>18/mn>/mmultiscripts>/math>

R. J. Charity, K. Brown, T. Webb, and L. G. Sobotka

Phys. Rev. C **107**, 054301 — Published 2 May 2023

DOI: 10.1103/PhysRevC.107.054301

Invariant-mass spectroscopy of ^{10}B, ^{11}C, ^{14}F, ^{16}F, and ^{18}Na

R.J. Charity,[1,*] K. Brown,[1,2] T. Webb,[3] and L.G. Sobotka[1,3]

[1] *Department of Chemistry, Washington University, St. Louis, Missouri 63130, USA*
[2] *FRIB Laboratory, Michigan State University, East Lansing, Michigan 48824, USA*
[3] *Department of Physics, Washington University, St. Louis, Missouri 63130, USA*

(Dated: April 6, 2023)

The invariant-mass method is used to study the structure of a number of light proton-rich isotopes utilizing fast beams. Reactions where the projectile picks up a proton have been used to study d-wave resonances in ^{14}F, ^{16}F, and ^{18}Na. While the ^{16}F and ^{18}Na results are consistent with previous studies, the ^{14}F results are not consistent with the only previous work. We have tentatively identified the 4^+ member of a rotational band in ^{10}B, which is the analog of well-known states with strong α-cluster structure in ^{10}Be and ^{10}C. Finally, spin and parities of newly observed states in ^{11}C which decay sequentially into three-body exit channels have been determined or restricted.

I. INTRODUCTION

The invariant-mass method is a powerful tool allowing one to explore nuclear states in the continuum. This technique is especially useful for exploring the spectroscopy of nuclei beyond the drip lines where all levels are unbound. In this work, we show examples of invariant-mass spectroscopy in light nuclei using the data from two experiments.

Nucleon pickup reactions with fast beams are very selective. Due to the mismatch of energy and momentum in the transfer of a nucleon from a target orbital to a projectile orbital, projectile orbitals with low orbital angular momentum are strongly disfavored [1–5]. Therefore, in *sd*-shell nuclei, such transfers favor nucleon placements into the d orbitals as compared to the $s_{1/2}$ orbital. In this work we will look at proton transfer reactions with beam nuclei located just inside of the proton drip line creating states in nuclides located near or just beyond this line. Beams of ^{15}O and ^{17}Ne are used to study levels in ^{16}F and ^{18}Na which are well known. With insight gained from these cases, we will then look at proton transfer with a ^{13}O beam creating ^{14}F for which only one previous study has been made [6]. Our results show some inconsistencies with this previous work.

The nucleus ^{10}Be is well known for having a highly-deformed rotational band associated with strong α-cluster structure where the two valance neutrons occupy molecular-like orbitals [7]. The analog of this band has recently been identified in the mirror nucleus ^{10}C [8]. Another analog of this band should be found in the T=1 states of ^{10}B. We expect the higher-lying members of this band to α decay to the isobaric analog state in ^{6}Li which then decays by γ-ray emission [9]. Exit channels involving multiple particles and γ rays were also observed in our ^{16}F events. Methods to deal with such exit-channels will be discussed.

Spin assignments of observed states are usually accomplished using well-defined reaction mechanics. Measured quantities such as the ejectile's angular distribution in transfer reactions, or the momentum distribution of residual products in nucleon knockout reactions are compared to theoretical predictions assuming transfer/knockout associated with specific orbitals. While the invariant-mass technique has been used for these specific reactions, the invariant-mass method can also be used for many other more complicated reactions where theoretical methods are not developed.

It would be useful to have some reaction-independent method for spin determination. Unfortunately this is not possible for two-body exit channels, but with three or more final products, information on the parent's spin/parity can be obtained from their momentum correlations. One recent example of this is the identification of the second 0^+ state in ^{10}C which was observed to decay by prompt $2p$ emission [8]. The observed proton correlations were found to be identical to those for ^{12}O and ^{16}Ne ground-state $2p$ emitters allowing the spin to be determined. In this work we will look at three-body exit channels associated with sequential decay through a well characterized intermediate state. In particular, we will study sequential proton and α decays of a number of ^{11}C states. For one of these states, the spin/parity is uniquely determined from the correlations, while for other states there is some restriction on the possible values.

II. EXPERIMENTAL METHODS AND ANALYSIS

The experimental data were obtained using fast secondary beams produced at the Superconducting Cyclotron Laboratory at Michigan State University. In all cases, the secondary beams were incident on the same 1–mm-thick ^{9}Be target and the decay products were detected in the High Resolution Array (HiRA) [10] with nearly identical configurations covering the same angular regions of the decay products (≈2°-12°). In these experiments, HiRA consisted of 14 Si-CsI(Tl) $E-\Delta E$ telescopes. Each telescope contained a double-side Si strip detector which provided position (scattering angle) information and behind this was placed a 2×2 array of CsI(Tl)

* charity@wustl.edu

crystals. This arrangement allowed for multi-hits in the same telescope to be identified and thereby dramatically increased the detection efficiency.

Results from two separate experiments are presented and in both cases aspects of these data concerning other nuclides have already been published. The first experiment utilized a mixed ^{15}O (≈89%, E/A=48.1 MeV) plus ^{17}Ne (≈11%, E/A=58.2 MeV) secondary beam [5, 11–14] while the second experiment used a ^{13}O secondary beam of E/A=65.4 MeV [15–19]. See the listed references for more details.

For the ^{15}O/^{17}Ne experiment, the γ-ray array CAESAR (CAESium iodide ARray) [20] surrounded the target to detect any γ rays in coincidence with the charged particles. For these experiments, the array consisted of 158 CsI(Na) crystals covering the polar angles between 57.5° and 142.4° in the laboratory with complete azimuthal coverage. The first ring and the last two rings of the full CAESAR array were removed due to space constraints.

For exit channels where there is a heavy residue, superior invariant-mass resolution can be achieved by selecting events where this residue is recoiled perpendicular to the beam direction [5, 14]. Let θ_H be the recoil angle of the heavy residue in the parent's reference frame with respect to the beam axis. When gates on $\cos\theta_H$ are used, they will be specified in the figure captions.

If the mass of the ground state is well known, then this quantity is subtracted from the deduced invariant mass to give distributions of the excitation energy E^*. For some excited states there is the possibly of emitting a γ ray in the decay process. However, the energy of γ rays is not included in our invariant-mass determination, and after subtracting the ground-state mass, we have designated the resulting quantity as $E^*_{n\gamma}$ in such cases. For events where there is no γ ray emitted, then $E^*_{n\gamma}$ is just the excitation energy. Otherwise this quantity represents the excitation energy reduced by the total γ-ray energy. In the cases of ^{18}Na→ p+^{17}Ne and ^{14}F→ p+^{13}O decays, the results are presented in terms of the proton decay energy Q_p instead.

Fits to the invariant-mass spectrum are made using either Breit-Wigner or R-matrix [21] intrinsic line shapes for the identified resonances. In some fits, these peaks are assumed to sit atop a smooth background which are typical parameterized as a polynomial times an inverse Fermi function. The effect of the detector resolution and decay-energy-dependent efficiency are incorporated via Monte Carlo simulations [5]. The latter include the angle and energy acceptance of the telescopes, the energy loss and small-angle scattering of the decay products in the target material and the angular and energy resolutions of the detector elements.

Uncertainties listed for the centroids in the following tables are only statistical. Systematic uncertainties are estimated from fitting invariant-mass spectra of well-known narrow states [9] with exit channels containing similar particle-types. The deviation of the fitted centroids from the tabulated values is at most 20 keV and we take this extreme value as our systematic uncertainty.

Fitted widths of the resonances can be compared to single-particle estimates obtained with a potential model. The potential we use has a Wood-Saxon form factor with standard parameters: r=r_{so}= 1.26 fm, a=a_{so}=0.6 fm, and V_{so}=6.4 MeV. The depth of the Wood-Saxon is adjusted to reproduce the experimental decay energy.

III. PROTON PICKUP

A. ^{16}F

The nuclide ^{16}F has 4 states with excitation energy below 1 MeV with a gap of 3 MeV to the next higher-lying levels. These four low-lying states are well described as particle-hole excitations on a ^{16}O core [22]. The lower two resonances (0^-, 1^-) are largely $^{15}\mathrm{O}_{g.s.} \oplus \pi(s_{1/2})$ in character while other two states (2^-, 3^-) are largely $^{15}\mathrm{O}_{g.s.} \oplus \pi(d_{5/2})$.

These levels were investigated using detected ^{15}O+p events produced with the mixed ^{15}O/^{17}Ne beam. The distribution of the reconstructed laboratory velocity of the ^{16}F parent, shown in Fig. 1(a), has two peaks. The higher-velocity peak has a maximum at the velocity of the ^{17}Ne beam component (see arrow) and ^{16}F states can be produced by the knockout of one proton from the ^{17}Ne projectile or via sequential decay of inelastically excited beam particles. The lower-velocity peak is associated with proton transfer to the slower ^{15}O beam component and, as expected for this process, the reconstructed ^{16}F velocities are below velocity of the ^{15}O beam component (see arrow).

The excitation-energy distributions determined from the invariant-mass method for the two beam components separated based on their parent velocities are plotted in Figs. 1(b) and 1(c). Reactions induced with the ^{17}Ne beam populate all four of the ^{16}F states with significant yields in Fig. 1(b). However, we note that the experimental spectrum actually has five peaks. There are a number of processes that contribute to the detected ^{15}O+p pairs:

(i) The prompt knockout of a proton from a ^{17}Ne projectile produces a ^{16}F resonance. There will contributions to the detected ^{15}O+p yield where either the first prompt proton or the second delayed proton from the decay of the resonance is detected. The former of these is expected to produce a smooth background.

(ii) Direct knockout of two protons from a ^{17}Ne projectile, but only one is detected again producing a smooth background component.

(iii) Sequential 2p decay of a ^{17}Ne resonance produced in the inelastic excitation of a beam particle. If only the first of these protons is detected, then this can produced a spurious peak. However, if the second

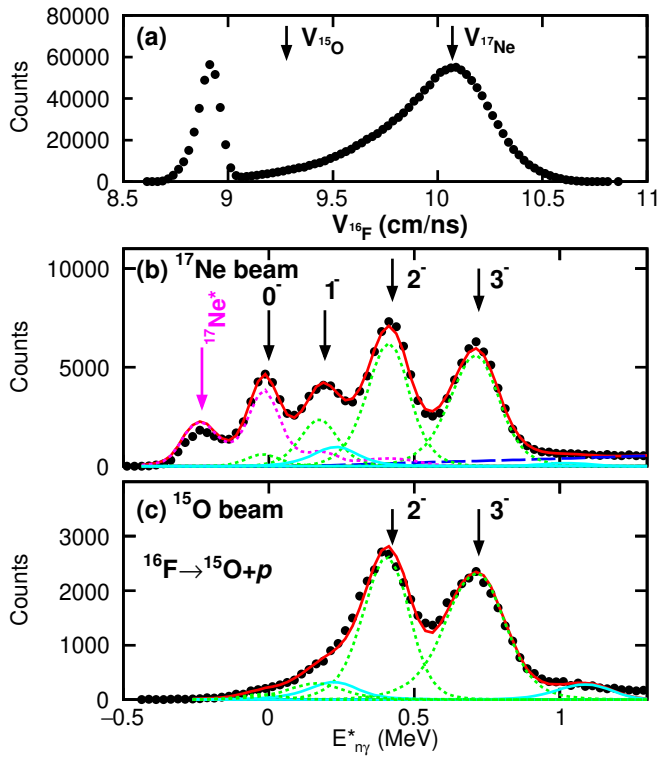

FIG. 1. Results from an invariant-mass study of ^{15}O+p events produced with the mixed ^{15}O/^{17}Ne beam. (a) Laboratory velocity distribution of the reconstructed ^{16}F parents. For comparison, the arrows show the velocities of the two beam components taking into account their energy loss in traversing 1/2 the target thickness. (b, c) Distributions of the ^{16}F excitation-energy quantity $E^*_{n\gamma}$ gated on the two beam components. To improve resolution only $|\cos\theta_H| < 0.2$ events are histrogrammed. Red curves show joint fits to these distribution including contributions from the four low-lying states at their tabulated widths (dotted green curves). The dotted magenta curve in (b) shows the contribution from inelastically scattered ^{17}Ne fragments (E^*=1.749 and 2.65 MeV) that undergo sequential two-proton decay. Appropriately scaled components with ≈5.2-MeV gamma rays in the exit channel are shown in (b) and (c) (cyan curves). For these components the invariant-mass deduced energy $E^*_{n\gamma}$ is less than the total excitation energy by the gamma-ray energy. The dashed blue curve in (c) is the background from promptly emitted protons and the dotted green curves show contributions from individual levels

protons is detected, then this adds to the yield of the ^{16}F peaks.

The spurious peak at negative excitation energy can be traced to the excitation of the E^*=1.749-MeV 5/2$^-$ state of ^{17}Ne which decays through the 0$^-$ ground state of ^{16}F as was deduced from this data set in Ref. [23]. Using the simulation from that work, the yield of detected ^{15}O+p events from the decay of this state is shown by the dotted magenta curve where its magnitude is normalized based on the yield of this peak in the detected ^{15}O+2p events. In addition to the 5/2$^-$ state, the dotted magenta curve also includes a smaller contribution from the E^*=2.65-MeV ^{17}Ne level [9] which sequentially decays through the 2$^-$ level of ^{16}F. This ^{17}Ne level is also prominent in the ^{15}O+2p invariant-mass spectrum. However, higher-lying ^{17}Ne states are wider and difficult to separate from the background of process (ii) in the ^{15}O+2p invariant mass spectrum. They should produce very wide spurious peaks which when combined would contribute to a smoother background under the ^{16}F peaks but we are unable to predict this contribution at present. The dotted magenta curve from the lower two ^{17}Ne states does explain all the yield of the spurious peak at negative excitation and most of the yield of the peak associated with 0$^-$ ground state of ^{16}F.

The shape of the background from the prompt protons in processes (i) and (ii) can be estimated from Ref. [24] using event mixing. The dashed blue curves in Fig. 1(b) shows this distribution where its magnitude has been normalized to the high-energy tail of the distribution. Its contribution to the detected events is quite small though possibly some of the wide spurious background also contributes to the tail region as well which would make this component even smaller.

The proton configuration of ^{17}Ne is known to have significant $(s_{1/2})^2$ and $(d_{5/2})^2$ components [25, 26] and thus, following the knockout of one these protons, we can expect both $s_{1/2}$ and $d_{5/2}$ ^{16}F resonances to be populated explaining a significant fraction of the yield in the other observed ^{16}F peaks.

While the distribution from the ^{17}Ne beam component is complicated, the spectrum from the ^{15}O beam component should be much simpler with no spurious peaks and no background from prompt protons. Also given the selectivity of proton-pickup reactions, we expect the 2$^-$ and 3$^-$ d-wave resonances to be more strongly populated in the pickup reaction [Fig. 1(c)]. This is indeed correct and in fact there is little discernible yield for either of the two s-wave resonances. This observation confirms the structure of these ^{16}F states and shows the high degree of selectivity of pickup reactions at these bombarding energies.

Detected ^{15}O+p events from both beam components contain, in addition to proton decays to the ground state of ^{15}O, the possibility of proton decays to excited states in ^{15}O which γ decay. The γ-ray energy spectrum measured in coincidence with these events is shown in Fig. 2(a). This spectrum is Doppler corrected for the measured velocity vector of the ^{15}O fragment and addback from neighboring crystals has been implemented [20]. Of particular interest is the unresolved E_γ=5.183/5.241-MeV doublet for which the full-absorption and the first-escape peaks are visible. The dotted vertical lines shows the gate used to select these γ rays and the coincident $E^*_{n\gamma}$ excitation energy spectrum are the red data points in Fig. 2(b). The known γ-ray peaks sit on a background which is also present in our gate. Based on past experience, the $E^*_{n\gamma}$ distribution associated with the γ background has largely the

TABLE I. Comparison of the fitted level parameters for ^{16}F from this work and the recent evaluated values from Stefan *et al.* [22]. The uncertainties listed for the centroids are statistical only. While we have estimated an overall systematic error of 20 keV for all channels, the deviation of our fitted centroids from their known values is smaller for this channel.

	This Work				Evaluated	
J^π	Q_p	$E^*_{n\gamma}$	E^* [a]	Γ	$E*$	Γ
	(MeV)	(MeV)	(MeV)	(keV)		
0^-	0.518(9)	-0.013(9)	-0.013(9)	25.6(46) [c]	0	25.6(46)
1^-	0.715(9)	0.184(9)	0.184(9)	76(5) [c]	0.194(5)	76(5)
2^-_1	0.951(6)	0.421(6)	0.421(6)	5.0(20) [c]	0.424(5)	5.0(20)
3^-_1	1.248(9)	0.717(9)	0.717(9)	15.1(67) [c]	0.721(4)	15.1(67)
(3^+)	0.773(7)	0.242(7)	5.483(7)[b]	65(28)		
	1.594(45)	1.063(45)	6.304(45)[b]	10(70)		

[a] Excitation energy calculated based on the AME2020 ground-state mass [27].
[b] Excitation energy calculated based on proton decay to $5/2^+$ state in ^{15}O.
[c] Not fit,taken from from the evaluation of [22] and used to fine tune experimental resolution.

same shape as the ungated $E^*_{n\gamma}$ spectrum. The background spectrum shown in Fig. 2(b) by the blue square data points is a scaled version of this, where the scaling factor is chosen to remove all features associated the 0^-, 1^-, 2^-, and 3^- states which decay to the ground state. Background-subtracted spectra, now gated on the two beam components, are shown as the data points in Fig. 3.

These spectra are quite different from the ungated distributions and shows the presence of two new levels. A joint fit was performed on the invariant-mass spectra from both beam components with and without the γ-ray gate. Breit-Wigner line shapes were assumed for all resonances with the effects of the experimental resolution incorporated via Monte Carlo simulations [5]. The experimental resolution was fine tuned in these simulations to reproduce the experimental widths of the peaks for the 0^-, 1^-, 2^-, and 3^- states with the intrinsic widths constrained to the values from the recent compilation of Ref. [22]. The two new levels contribute to both the spectra with and without the γ-ray gate, the magnitude in the latter is scaled to correct for the predicted γ-ray efficiency for the gate used as calculated from a GEANT4 simulation [28, 29]. For the spectrum from the ^{17}Ne beam component in Fig. 1(b), contributions from sequential decay (dotted magenta curve) and prompt protons (dashed blue curve) have been included in the fits.

Excitation energies listed in Table I are calculated based on the AME2020 [27] ground-state mass for ^{16}F. The excitation energy of the 0^- ground-state peak is very close to zero and the values for the other peaks are consistent with the systematics of [22] also listed in the table. The excitation energies listed for the new states are based on their decay to the 5.241-MeV $5/2^+$ state in ^{15}O. If decay is to the 5.183-MeV $1/2^+$ state instead, then the excitations energies would be 58 keV lower. In understanding the structure of the new levels, we note the following points.

(a) The reaction mechanism for the production of these resonances with the ^{17}Ne beam component is not entirely clear. There are the possibilities of producing them via proton knockout reactions or in the sequential $2p$ decay of inelastically excited ^{17}Ne projectiles. For the latter, no narrow ^{17}Ne level could be identified in the ^{15}O+$2p$+γ data that could feed these states, but contribution from unresolved wider states might be possible. For the simplest incarnations of these two processes, such as single-step proton knockout, the distribution of the reconstructed ^{16}F parent velocity is expected to have a peak near the ^{17}Ne beam velocity. A comparison of the velocity distribution for the two $d_{5/2}$-wave resonances (red curve) and the lowest-energy new state at $E^*_{n\gamma}$=0.249 MeV (black data points) is made in Fig. 4. The latter is background subtracted and corrected for the efficiency of the γ-ray gate. The distribution for the $d_{5/2}$-wave resonances is peaked close to the ^{17}Ne beam velocity and its shape is only slightly asymmetric about this value. This distribution probably is dominated by single-step proton knockout. However the low-velocity tail causing this asymmetry is likely due to more complicated multi-step processes. In contrast, the distribution for the new level is concentrated in the tail region suggesting the observed yield is most likely from multi-step processes.

(b) For proton pickup, the yields of the new peaks are small compared to those from the 2^- and 3^- states even after correcting for the γ-ray efficiency. See Fig. 1(c) where the efficiency-corrected yield for the new levels are shown by the solid cyan curve. The total yield of these states might be larger due to proton decay branches to $^{15}O_{g.s.}$, but the low efficiency and bad resolution of the array for such high-energy proton-decay events give us

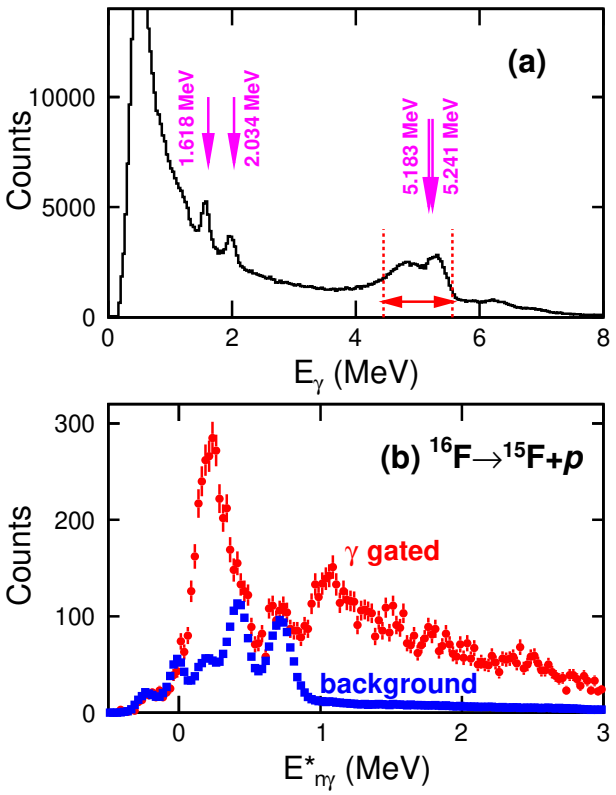

FIG. 2. (a) Doppler-corrected spectrum of γ-ray energies found in coincidence with the ^{15}O+p events from both beam components. The location of some known ^{15}O γ rays are indicated with the arrows. The gate used to select events associated with the E_γ=5.183/5.241-MeV doublet is indicated. (b) Spectrum of the ^{16}F excitation-energy quantity $E^*_{n\gamma}$ in coincidence with the E_γ=5.183/5.241-MeV γ-ray doublet and for $|\cos\theta_H| < 0.2$ is shown by the red data points. The blue data points are an estimate of the background obtained from downscaling the ungated excitation spectrum.

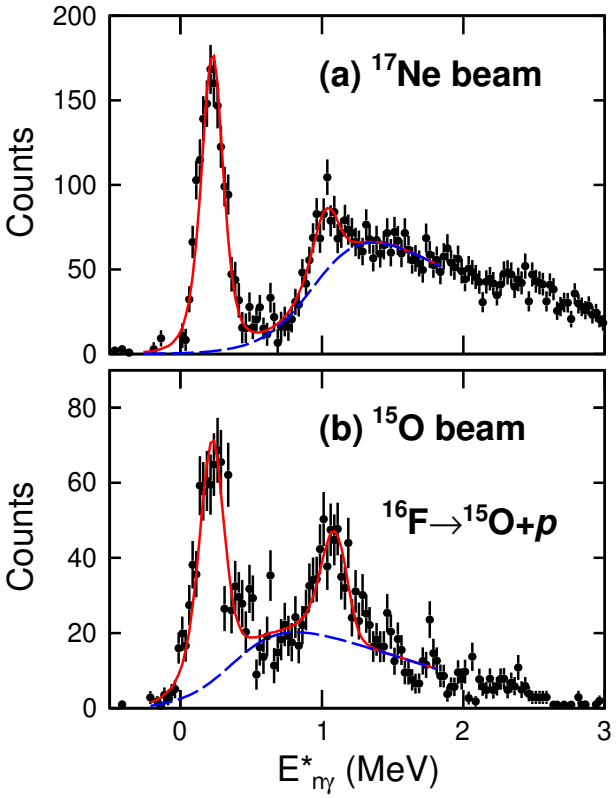

FIG. 3. Distributions of the background-subtracted excitation-energy quantity $E^*_{n\gamma}$ for events in coincidence with the E_γ=5.183/5.241-MeV γ-ray doublet and for $|\cos\theta_H| < 0.2$. Panel (a) is associated with reactions produced by the ^{17}Ne beam component while panel (b) is for the ^{15}O beam component.

almost no sensitivity to such branches. However, the spectroscopic factor for the latter decays cannot be large as the measured decay widths in Table I are small. For example in our potential model, the $d_{5/2}$ and $f_{7/2}$ single-particle decay widths of the $E^*_{n\gamma}$=0.249-MeV level to the ground state are 2.7 and 0.55 MeV, respectively. These are much larger than the experimental value of 65(28) keV.

(c) Even with very small spectroscopic factors, the production of these resonances in the pickup reaction can be enhanced if the picked-up protons are captured into even higher ℓ orbits ($\ell > 2$) where the effects of momentum mismatch are not as severe as they are for the d-wave resonances.

If a $f_{7/2}$ proton were picked up by the J^π=1/2$^-$ ^{15}O ground state, then J^π=3$^+$ and 4$^+$ states can be produced in ^{16}F. To produce 3$^+$ and 4$^+$ states via a single-step proton knockout from the J^π=1/2$^-$ ^{17}Ne projectile would require removing an f-wave or even higher ℓ-wave proton. However, as we expect negligible spectroscopic strength for such orbits in the ground-state of ^{17}Ne, the production of the proposed 3$^+$ and 4$^+$ states with the ^{17}Ne projectile would require more complex multi-step processes consistent with our interpretation of Fig. 4. Comparing the level schemes of ^{16}F and its mirror ^{16}N in Fig. 5, we see a second 3$^+$ state is expected in ^{16}F close to the energy of our new $E^*_{n\gamma}$ = 0.249-MeV state, suggesting it is the analog of our new state. In Fig. 5, the ^{16}N levels are shifted so that the two $d_{5/2}$ resonances (2$^-$, 3$^-$) line up in both mirror systems. Relative to these reference levels, the $s_{1/2}$ resonances (0$^-$, 1$^-$) are shifted down by ≈600 keV in ^{16}F, a classic Thomas-Erhman shift. The proposed 3^+_2 state in ^{16}F does show a small downward shift with respect to it possible mirror of 163(10) keV. This suggests a reduced proton $s_{1/2}$ strength compared to the 0$^-$ and 1$^-$ states.

Shell-model calculations with the OXBASH code [30] in *psd* space with the WBT and WBP effective interactions [31] predict that the first two 3$^+$ states have significant strength for both ^{15}O(1/2$^+$)$\oplus\pi(d_{5/2})$ and ^{15}O(5/2$^+$)$\oplus\pi(s_{1/2})$ configurations. For the second 3$^+$

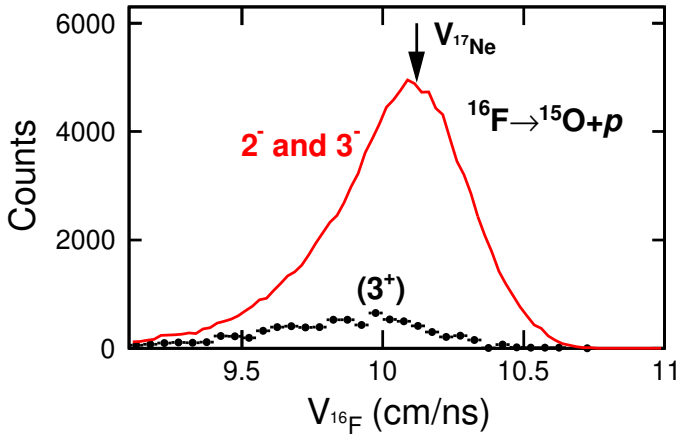

FIG. 4. Comparison of reconstructed velocity distributions of the ^{16}F parent for $d_{5/2}$-wave resonances (2^- and 3^-, red curve) to that for the newly observed level at $E^*_{n\gamma}$=0.249 MeV (black data points). The latter is background subtracted and corrected for the γ-ray efficiency. The arrow indicates the velocity of the ^{17}Ne beam component.

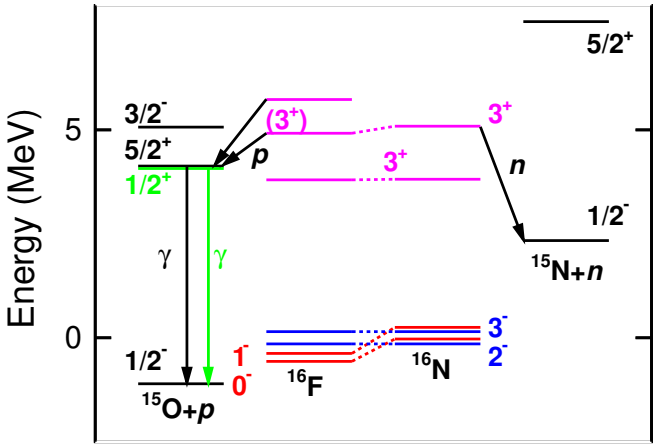

FIG. 5. Comparison of levels of interest in the mirror pair ^{16}F and ^{16}N including daughter levels associated with their decay. In order to highlight Thomas-Erhman shifts, the zero energy on the y-axis is based on the average of the 2^- and 3^- states, both of which lack significant proton (neutron) $s_{1/2}$ strength in ^{16}F (^{16}N). The two new states observed in this work have arrows showing their proton decay to the E^*=5.183/5.241-MeV double in ^{15}O.

state, the spectroscopic strengths are predicted to be 57(20)% and 38(9)%, respectively. Experimentally, more of the ^{15}O$(5/2^+)\oplus\pi(s_{1/2})$ strength appears to be associated with the second 3^+ state as the first has no noticeable Thomas-Erhman shift (Fig. 5). The width of the our proposed 3^+_2 state also suggests it is not a pure ^{15}O$(5/2^+)\oplus\pi(s_{1/2})$ configuration as this gives a single-particle decay width of 106 keV which is about two times larger than the experimental value.

TABLE II. Comparison of the fitted level parameters for ^{18}Na from this work to those from Assié *et al.* [33]. The uncertainties listed for centroids in this work are statistical only. A 20-keV systematic uncertainty is estimated.

	This Work		Assié *et al.*	
J^π	Q_p (MeV)	Γ (keV)	Q_p (MeV)	Γ (keV)
2^-_1	1.527(25)	22±100	1.552(5)	5(3)
3^-_1	2.085(23)	84(46)	2.084(5)	42(10)

B. ^{18}Na

The spectroscopy of ^{18}Na levels was investigated using detected ^{17}Ne+p events produced with the mixed ^{15}O/^{17}Ne beam. There was no evidence in the coincident γ-ray spectrum for proton decays to the first-excited state of ^{17}Ne, the only excited state of ^{17}Ne which γ decays. The velocity distribution of reconstructed ^{18}Na fragments is plotted in Fig. 6(a) and most events are located in a peak with velocity below that of the ^{17}Ne beam component as expected for proton pickup. The yield of events with velocities above this peak are attributed to some residual random coincidences events which were greatly suppressed by the application of coincidence time gates. Only events in main peak were used to construct the invariant-mass spectrum.

The nuclide ^{18}Na has been investigated in only a few experimental studies [32–34]. The inferred structure of the observed low-lying states is based on shell-model calculations [33, 35] which predict strong single-particle configurations coupled to the ^{17}Ne ground ($1/2^-$) and first excited state ($3/2^-$). In these calculations, there are two states (0^-_1, 1^-_2) of ^{17}Ne$(1/2^-)\oplus\pi(s_{1/2})$ character, two more states (2^-_1, 3^-_1) of ^{17}Ne$(1/2^-)\oplus\pi(d_{5/2})$ character, and another two states (1^-_1, 2^-_2) of ^{17}Ne$(3/2^-)\oplus\pi(d_{5/2})$ character. The 2^-_1 and 3^-_1 states of ^{17}Ne$(1/2^-)\oplus\pi(d_{5/2})$ character should be the dominate levels populated in proton transfer reactions.

The experimental ^{18}Na decay energy (Q_p) spectrum plotted in Fig. 6(b) indeed shows two peaks located close to the energies for these states deduced in the proton-elastic-scattering study of Assié *et al.* [33] (see arrows). The red curve shows a two-level fit using Breit-Wigner intrinsic line shapes. The fitted energies and widths are compared to the values from Assié *et al.* in Table II and are found to be consistent.

C. ^{14}F

The nuclide ^{14}F has been observed in only one previous study which utilized proton elastic scattering [6]. An R-matrix fit of their measured excitation function was

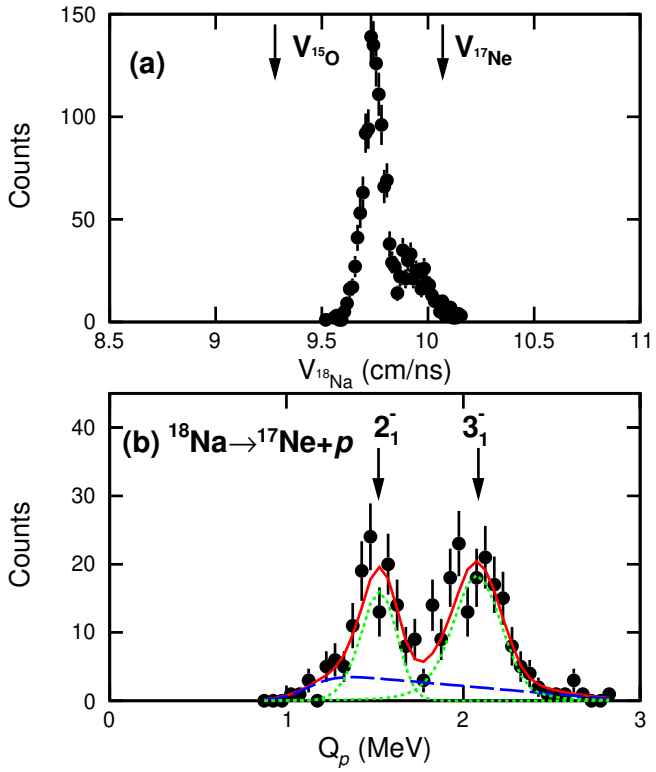

FIG. 6. Results from the invariant-mass study of ^{17}Ne+p events produced with the mixed ^{15}O/^{17}Ne beam. (a) Laboratory velocity distribution of the reconstructed ^{18}Ne parents. For comparison, the arrows show the velocities of two beam components in the center of the target. (b) ^{18}Na decay-energy distributions. To improve resolution only $|\cos\theta_H| < 0.2$ events are histrogrammed. The red curve is a fit to this distribution with two levels of Breit-Wigner intrinsic line shape (dotted curved curves) plus a smooth background component (dashed blue curve). The arrows indicate the energies of the 2^-_1 and 3^-_1 states from Assié *et al.* [33].

interpreted as containing two ≈1-MeV wide s-wave resonances (2^- and 1^-) at low energies. Above these states, two narrower d-wave resonances (3^- and 4^-) were found. Based on experience with the previous pickup reactions, we would only expect to observe the two d-wave resonances in proton transfer to ^{13}O. For ^{13}O, we expect a breakdown of the Z=8 shell closure due to the intruder $1s_{1/2}$ orbital based on results obtained with the mirror ^{12}Be nucleus [36–38]. Thus ^{13}O has significance proton $(0p_{1/2})^2$ and $(1s_{1/2})^2$ configurations for the valence protons.

The velocity distribution of reconstructed ^{14}F fragments obtained from detected ^{13}O+p events with the ^{13}O beam, shown in Fig. 7(a), has a narrow peak located below the beam velocity similar to that observed in the other proton pickup reactions. The ^{14}F decay energy spectrum is displayed in Fig. 7(b) and 7(c). These represent proton decays to the ground state as ^{13}O has no particle-stable excited states. There are no resolved peaks at the reported energies of the d-wave resonances (3^- and 4^-) indicted by the arrows in this figure. Rather the most prominent peak is located in between these values. Indeed the region 3.12< Q_p(MeV) <3.6 containing this prominent peak corresponds to a region in the excitation function of Ref. [6] which was deemed to be distorted and possibly less sensitive to such a level. In a simple potential model, Sherr and Fortune [39] looked for consistency with this previous work and suggested the 3^- state was actually located in this distorted region at Q_p=3.65 MeV close to the energy of our observed peak. Our data thus supports this contention. Below the main peak in the invariant-mass spectrum [1.5< Q_p(MeV) <2.5] sits a plateau structure which is probably associated with one or more wide states. Its existence is surprising as only the $s_{1/2}$-wave resonances (2^- and 1^-) were found in this region in Ref. [6] and these should not be produced significantly in the proton pickup reaction (see Sections III A and III B). Possibly one or more of these states have significant $d_{5/2}$ strength in addition to the $s_{1/2}$ strength.

The largest uncertainty in extracting the parameters of the new peak is due to the parameterization of the background of unresolved resonances on which it sits. We have made two fits with different assumptions to gauge the sensitivity to this parameterization. The fit shown in Fig. 7(b) was obtained with three wide peaks and no other background where all peak parameters are allowed to vary. Three is the minimum number of peaks that can produce a good fit to our data. Tabulated peak parameters are listed in Table III. As the peaks are wide, we have used R-matrix intrinsic line shapes [21] where the listed Q_p and Γ values are associated with energies of the maximum in the intrinsic line shape and their FWHM values, respectively. Already there is tension, as to fit the plateau region, the lower-energy peak must be consider as a pure $s_{1/2}$ resonance, which should not be excited significantly. However, the other two peaks are fitted as d-wave resonances. The fit parameters of the most prominent new peak, possibly the 3^- state, are Q_p=3.511(14) MeV and Γ=0.74(5) MeV where the quoted uncertainties are just statistical from the fitting procedure.

In the second fit, shown in Fig. 7(c), in addition to the new peak, contributions from four states whose parameters (Q_p and Γ) are fixed to the values deduced in [6] were allowed. However in order to get a good fit, an additional smooth background (parameterized as an inverse Fermi function times a first-order polynomial) was necessary. The best fit had no contributions from the 3^- state of Ref. [6] and the fitted smooth background is small. The fitted parameters of the new peak are now Q_p=3.569(14) MeV and Γ=0.89(1) MeV. Including both fits and the systematic uncertainty associated with Q_p, the final parameters are Q_p = 3.54(6) MeV and Γ=0.80(9) MeV. At this decay energy, the single-particle decay width is $\Gamma_{s.p.}$=0.54 MeV, implying a spectroscopic factor of C^2S=1.6(1) and thus it represents a good single-particle d-wave resonance.

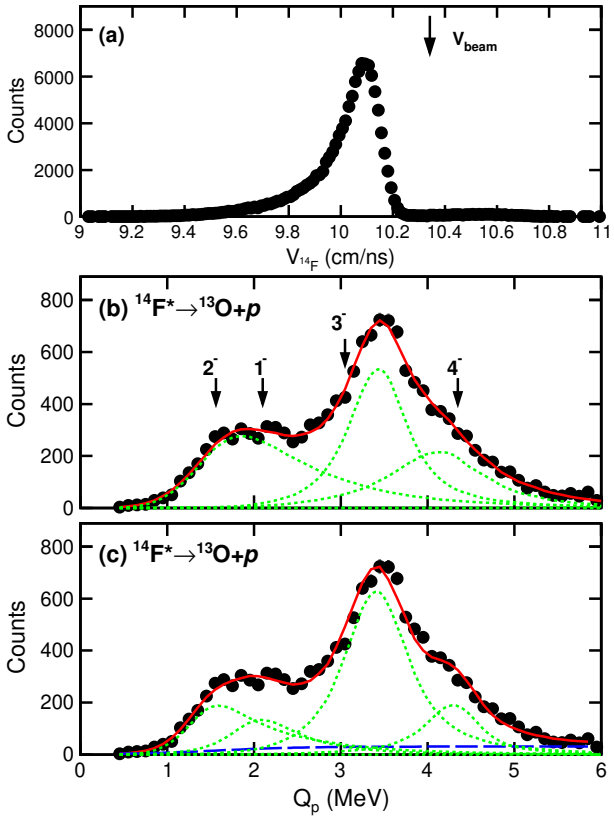

FIG. 7. Results from an invariant-mass study of ^{13}O+p events produced with the ^{13}O beam. (a) Laboratory velocity distribution of the reconstructed ^{14}F parents. For comparison the arrow shows the velocity the beam after traversing 1/2 the target thickness. (b, c) Experimental ^{14}F decay-energy distributions are given by the data points. To improve resolution only $|\cos\theta_H| < 0.5$ events are used to construct these. The red curves show fits to this distribution including only contributions from (b) three and (c) five levels. Fitted contributions from individual levels are shown by the dotted green curves and in panel (c) a smooth background (dashed blue curve) was necessary to improve the fit at the largest Q_p values. The deduced states from proton scattering study [6] are indicated by arrows in panel (b).

IV. ROTATIONAL BAND IN ^{10}B WITH T=1

The nuclide ^{10}Be is known for a highly deformed rotational band built on its second 0^+ state with strong α-cluster structure and where the two valance neutrons are located in molecular-like orbitals [7]. The band is known up to the 4^+ member and its moment of inertia is approximately 2.5 times greater than those for the ground-state bands of ^{8,9,10}Be. Recently, the analog band in the mirror nucleus ^{10}C has been identified up to the same spin, albeit with a tentative 4^+ state assignment [8]. To complete such information in the isobaric triplet, this band must be establish in the intermediate ^{10}B nucleus where these states will be at higher excitation energies.

The members of these bands in ^{10}Be and ^{10}C are known to have strong α+^{6}He or α+^{6}Be decay branches except for the band heads which are below threshold for these channels [7, 8]. The T=1, 0^+ state in ^{10}B is known at E^*=7.5599(4) MeV as is the 2^+ member of the band at E^*=8.895 MeV [9]. This latter 2^+ state and the 4^+ member, are expected to have strong branches to the ^{6}Li(IAS)+α exit channel. Here ^{6}Li(IAS), the isobaric analog of ^{6}Be and ^{6}He in ^{6}Li, decays to the ground state by emitting a 3.562-MeV γ ray [9]. We have searched for these ^{10}B states using the experimental data obtained with the ^{15}O/^{17}Ne beam where these states can be produced by multiple knockout of nucleons. The γ-ray spectrum obtained in coincidence with detected ^{6}Li+α events is plotted in Fig. 8(a) where one observes a full absorption peak associated with this γ ray and, less prominently at lower energies, its first-escape peak. Using the indicated gate in Fig. 8(a), the corresponding $E^*_{n\gamma}$ spectrum is shown in Fig. 8(b) as the black histogram. There are a number of prominent peaks visible which are associated with T=0 states [9] (see black arrows). These peaks are in coincidence with the background under the observed γ-ray peaks. As in Sec. III A, the shape of this background is taken from the ungated $E^*_{n\gamma}$ distribution and scaled to match the intensities of these T=0 peaks (green histogram). The background-subtracted spectrum is shown by the red histogram which displays two peaks (indicated by the red arrows).

Figure 9 shows a fit to this background-subtracted data with two Breit-Wigner intrinsic line shapes convoluted with the experimental resolution (green dotted curves) plus a smooth background (dashed blue curve). The fitted level parameters are listed in Table IV. The lower-energy peak, with fitted parameters of E^*=8.903(4) MeV, Γ=38(18) keV, is consistent with the 2^+ member of the rotational band which is listed at E^*=8.895(1) MeV and Γ=39(1) keV in the ENSDF data base [9]. A more recent study by Kuchera *et al.* constrained this peak as E^*=8.894(2) MeV, Γ=34(4) keV and finds a large reduced α decay width which confirms its expected strong α-cluster structure [40]. Our peak may also have contributions from the close by 3^- state at E^*=8.887(3) MeV which is also known to have a decay branch to the selected exit channel. However this state, which decays largely by proton emission [40], has a larger width of 96(4) keV [9] and thus cannot contribute

TABLE III. Level parameters from the three-peak fit to the ^{14}F decay energy spectrum of Fig. 7(b). Only statistical uncertainties are given.

J^π	Q_p	Γ
	(MeV)	(MeV)
(1^- or 2^-)	2.16(3)	1.16(2)
(3^-)	3.511(14)	0.74(5)
(4^-)	4.300(23)	1.21(5)

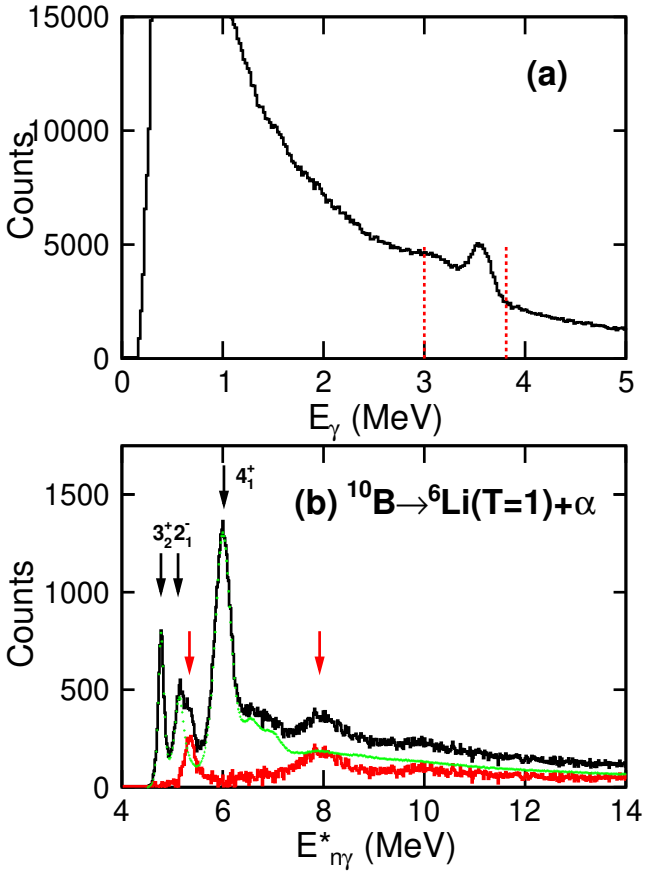

FIG. 8. Results from an invariant-mass study of ^{6}Li+α events produced with the mixed ^{15}O/^{17}Ne beam. (a) Spectrum of γ-ray energies recorded in coincidence with these events which have been Doppler corrected relative to the measured ^{6}Li velocity vector and addback from neighboring crystals has been implemented. The gate on the 3.563-MeV γ ray is indicated. (b) Distribution of the excitation-energy quantity $E^*_{n\gamma}$ with this γ-ray gate (black histogram). The contribution from the background events is shown as the green histogram. The background-subtracted spectrum is given by the red histogram. These excitation-energy spectra were produced with no gate on $\cos\theta_H$. The black arrows locate peaks associated with proton decay of known ^{10}B states to the ground state of ^{6}Li. The red arrows locate the peaks remaining after the background is subtracted.

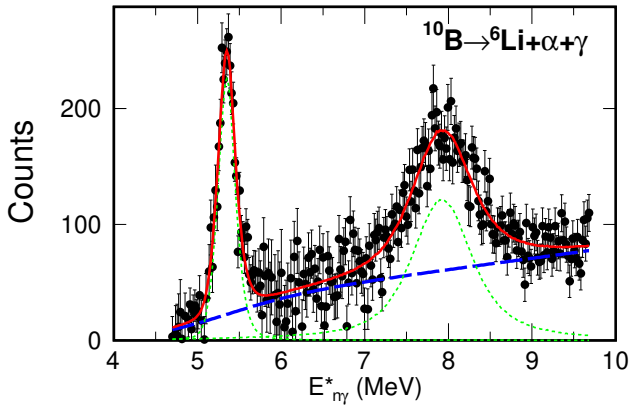

FIG. 9. Background-subtracted ^{6}Li+α+γ invariant-mass spectrum. The red curve shows the fit which contains two levels (green dotted curves) plus a smooth background (dashed blue curve).

significantly.

Kuchera *et al.* also suggested a 1^- spin assignment for a state observed in the α+^{6}Li(T=1) channel with E^*=11.63(7) MeV and Γ=480(150) keV [40]. This state is roughly consistent with our second peak in Fig. 9 for which we fit E^*=11.482(6) MeV ($E^*_{n\gamma}$=7.919 MeV) and Γ=538(61) keV. However these authors deduce a small decay branch to our selected exit channel, with the majority of the strength decaying to the p+^{9}Be$_{g.s.}$ channel with a large value of Γ_p/Γ_α=20(12). From our fitted α+^{6}Li(T=1) yield and the partial width from Kuchera *et al.*, the expected yield in the p+^{9}Be invariant-mass spectrum, taking into account our detector resolutions and efficiencies for both channels, is shown by the solid red curve in Fig. 10 where it is compared to our experiment data for this p decay channel. Clearly this expectation is grossly inconsistent with our data indicating that our state has a much stronger α+^{6}Li(T=1) decay branch and thus is not the J^π=1^- state assigned by Kuchera *et al.*. The state we observe has Γ_p/Γ_α less than 2.

Kirsebom *et al.* have also searched for the 4^+ member of the rotational band and tentatively assigned it to a state with E*=11.48(3) MeV and Γ=460(70) keV produced in ^{3}He+^{11}B→2α+^{6}Li reaction [41]. They identify the α+^{6}Li(T=1) decay channel from energy and momentum conservation without detecting the 3.563-MeV γ-ray. In addition they find $\Gamma_p/\Gamma_\alpha \lesssim$1.0. These results are consistent with our second peak in Fig. 9.

Assuming the 4^+ spin assignment, we compare the rotational bands of the isobaric triplet in Fig. 11. The excitation energies plotted here are relative to the first T=1, J^π=0^+ states. The energies of the same-spin members of the rotational bands line up quite well across the isobaric multiplet. The slopes for the bands built on the second 0^+ state, connected by the solid lines, are less steep than for those built on the first 0^+ state, verifying the larger moments of inertia for the former. There is a slight downward shift of the bands built on the second 0^+ with increasing proton richness. This is expected as the second 0^+ states have a significant $(s_{1/2})^2$ contribution for their valence nucleons giving rise to a downward Thomas-Erhman shift, decreased Coulomb energy with respect to states without this s component, when protons replace neutrons [8].

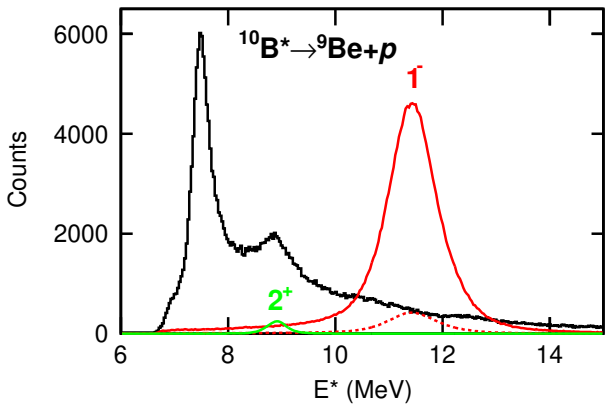

FIG. 10. Histogram shows the excitation-energy distribution determined from the invariant mass of ^{9}Be+p events. If the two peaks in our ^{6}Li+α+γ distributions are 2^+ and 1^- states, then from the branching ratios of [40] and our simulated detection efficiencies, their expected yields in the ^{9}Be+p channel are shown by the solid curves. The dashed red curve shows the maximum yield possible for the possible 1^- state.

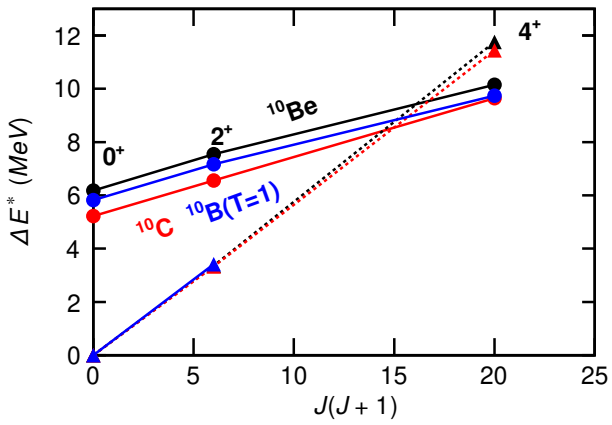

FIG. 11. Comparison of analog rotational bands in ^{10}C, ^{10}B, and ^{10}Be. The quantity ΔE^* is the excitation energy relative to the first T=1, J^π=0$^+$ state. The rotational bands built on these states have smaller moments of inertia compared to that for the second 0^+ states.

TABLE IV. Level parameters extracted from fitting the ^{6}Li+α+γ spectrum in Fig. 9. The errors listed for the centroids are statistical only and there is an additional 20-keV systematic uncertainty.

J^π	Q_p (MeV)	$E^*_{n\gamma}$ (MeV)	E* (MeV)	Γ (keV)
2^+	1.436(4)	5.340(4)	8.903(4)	38(18)
(4^+)	4.015(6)	7.919(6)	11.482(6)	538(61)

V. SPIN/PARITY DETERMINATION IN ^{11}C STATES

In this section we will discuss the method of spin assignment for three newly observed states in ^{11}C which decay by the sequential emissions of α particles and/or protons into the three-body exit channels; ^{6}Li+α+p and 2α+^{3}He. Before examining the ^{11}C invariant-mass distributions, let us consider the possible intermediate states in the decay. Figure 12(a) shows the excitation-energy distribution obtained from the ^{6}Li+α subevents of the detected ^{6}Li+α+p events where a number of peaks associated with possible ^{10}B intermediate states are visible. We could not find evidence for ^{11}C states with intermediate ^{6}Li+p or α+p resonances. The arrows in this figure show the location of known ^{10}B states [9] that decay nearly 100% to ^{6}Li+α except for the lowest 2^+ state shown which has only a 14% branching ratio to this channel. The lowest-energy peak observed in this distribution appears to arise solely from the 3^+ state in ^{10}B. The next two higher-energy peaks can have contributions from multiple ^{10}B states.

The ^{11}C→^{6}Li+α+p excitation energy distribution obtained from gating of the J^π=3$^+$ ^{10}B intermediate state is shown in Fig. 13 as obtained from the (a) ^{13}O and (b) ^{15}O/^{17}Ne data sets. The two data sets each display a narrow peak at E^* ≈14.1 MeV sitting on a broad distribution. The solid curves show fits with Breit-Wigner intrinsic line shapes and the fitted level parameters are listed in Table V. Consistent centroids and widths are obtained from the two data sets. Figure 14 shows the level and decay scheme.

Gating on the next higher-energy ^{10}B peak in Fig. 12 produces the ^{11}C excitation-energy distribution in Fig. 15 where a broad peak is present in both data sets. There is a low-energy shoulder below this peak which is probably associated with another level, but as it is not well resolved, we have incorporated its contribution into the smooth background in our fits. The fitted level parameters (Table V) are again consistent in the two data sets.

For the 2α+^{3}He exit channel, we only found evidence for ^{11}C states with ^{7}Be intermediate states. The ^{7}Be excitation-energy distribution from the α+^{3}He subevents (two for each 2α+^{3}He event) is displayed in Fig. 12(b) where the $7/2^-$ excited state is most prominent. The ^{11}C→2α+^{3}He excitation-energy distributions gated on this intermediate state is displayed in Fig. 16 for the two data sets. Both of these distributions are again similar to each other and also display peaks at E^* ≈14.1 MeV. The fitted level parameters are again listed in Table V and the centroids for this channel are only 30-40 keV larger than the lowest-energy level obtained in the ^{6}Li+α+p channel. However, this difference is above the systematic uncertainty of 20 keV. In addition it is clear that these are not two branches of the same state as the relative yields of these peaks in the two exit channels are different in the two data sets. The efficiency-corrected ratio of yields of the ^{6}Li+α+p to the 2α+^{3}He fitted peaks is 4.6(2)% for the ^{13}O data set compared to 9.5(4)% for the

TABLE V. Level parameters extracted from fitting the 2α+^{3}He and ^{6}Li+α+p exit channels. Results are shown for the experiments with the ^{13}O and ^{15}O/^{17}Ne beams. The uncertainties listed for the centroids are statistical only and there is an addition 20-keV systematic uncertainty.

		^{13}O beam			^{15}O/^{17}Ne beam	
J^π	channel	intermediate state	E^* (MeV)	Γ (keV)	E^* (MeV)	Γ (keV)
$7/2^+$	2α+^{3}He	^{7}Be ($7/2^-$)	14.102(2)	<190	14.102(2)	<230
$3/2^\pm$,$5/2^+$,$7/2^+$,$9/2^-$,$11/2^+$	^{6}Li+α+p	^{10}B (3^+)	14.130(10)	<92	14.142(5)	<108
$3/2^\pm$,$5/2^\pm$	^{6}Li+α+p	^{10}B ($2^\pm$)	16.083(10)	781(41)	16.167(25)	681(83)

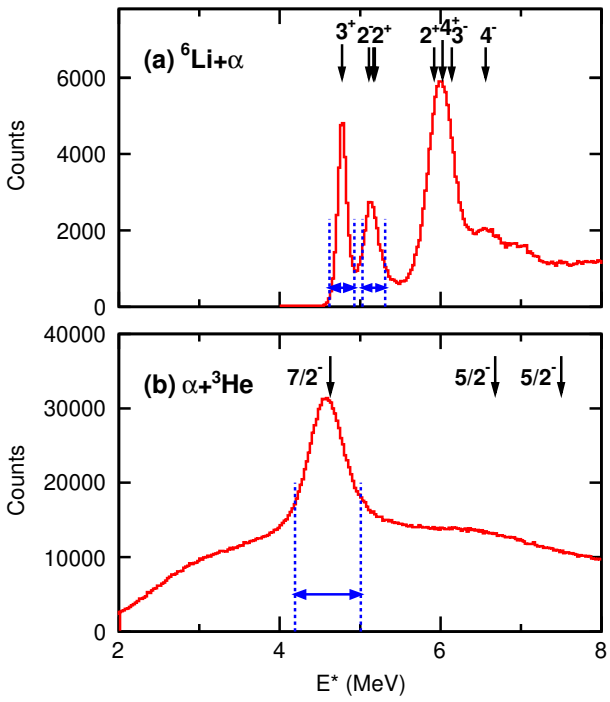

FIG. 12. Excitation-energy distributions obtained for intermediate states in the decay of ^{11}C parent states. Panel (a) is obtained from the ^{6}Li+α subevents of detected ^{6}Li+α+p events while panel (b) is for the two α+^{3}He subevents of detected 2α+^{3}He events. These data were obtained from the experiment with the ^{15}O/^{17}Ne beam. Gates are shown for which projected ^{11}C spectra are presented in Figs. 13, 15, and 16.

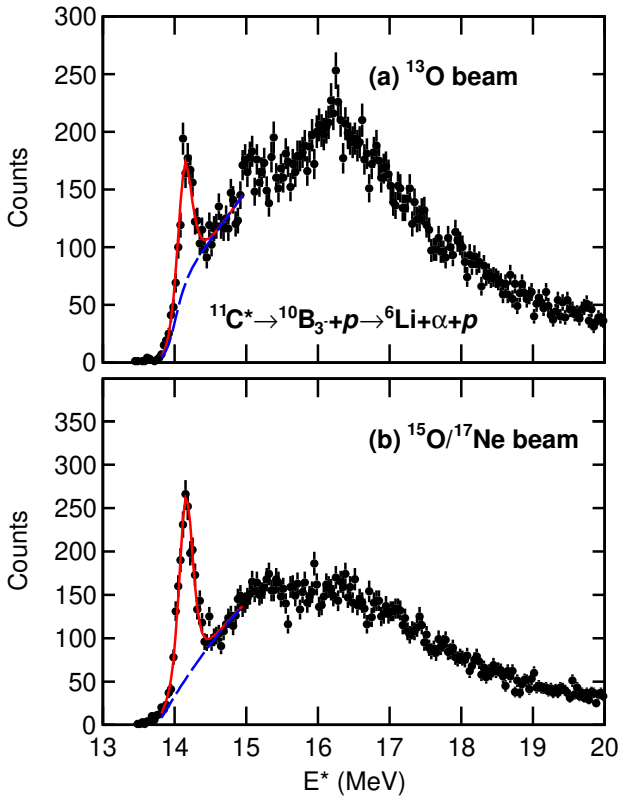

FIG. 13. Excitation-energy spectra for ^{6}Li+α+p events where there is a ^{10}B(3^-) intermediate state. Results shown were obtained with (a) ^{13}O and (b) ^{15}O/^{17}Ne beams. Fits to these data (solid red curves) are shown where the smooth fitted backgrounds are given by the dashed blue curves.

^{15}O/^{17}Ne data set.

Of the three new ^{11}C states observed in this work only the 14.1-MeV state, found in the 2α+^{3}He channel, is consistent with a known tabulated state in ^{11}C [9]. This previously known state is at E^*=14.070(20)-MeV and Γ=135(50) keV, with no spin-parity assignment. Information of the spin of the parent state in sequential decay can be obtained from the distribution of the angle $\theta_{1,2}$ between the two sequential decay axes. With an intermediate state identified, this angle is calculated event-by-event. Excitation-energy distributions similar to Figs. 13 to 16 were then created with extra gates on regions of $\theta_{1,2}$. From the fitted yields of the peaks, corrected for the $\theta_{1,2}$-dependent detector efficiency, the angular correlations in Figs. 17 and 18 were constructed. These can be compared to predictions using the theory of Refs. [42, 43].

The orbital angular momentum for proton decay of the 16.1-MeV state to ^{10}B must be either ℓ=0 or ℓ=1 in order to produce single-particle decay widths greater than

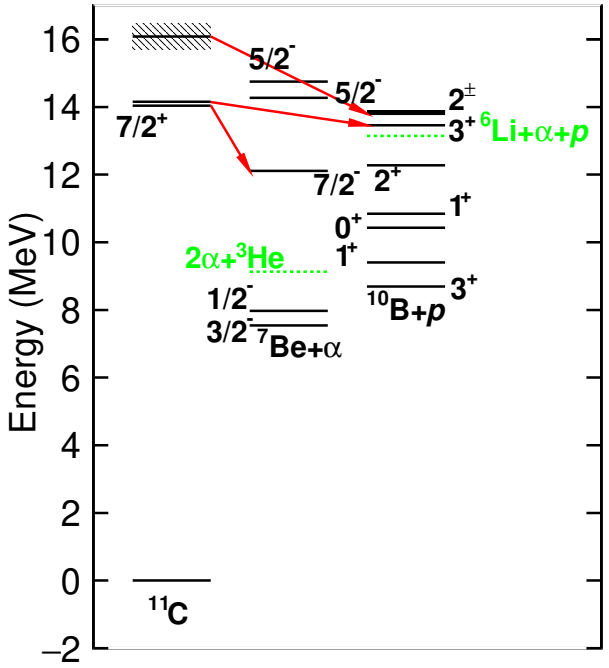

FIG. 14. Level scheme of ^{11}C showing the states observed in this work and their decay paths.

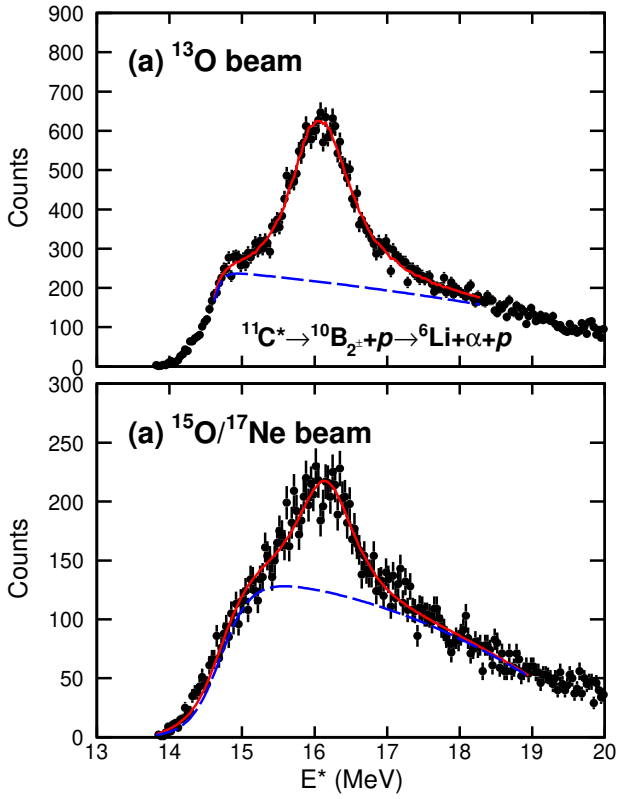

FIG. 15. Excitation-energy spectra for ^{6}Li+α+p events where there is a ^{10}B($2^{\pm}$) intermediate state. Results shown were obtained with (a) ^{13}O and (b) ^{15}O/^{17}Ne beams. Fits to these data (solid red curves) are shown where the fitted smooth backgrounds are given by the dashed blue curves.

or equal to the large experiment value. Proton $s_{1/2}$ and $p_{1/2}$ decays are both isotropic and consistent with the flat distribution observed in Fig. 17(b). We also considered parent J^π assignments consistent with $p_{3/2}$ proton emission, but the calculated angular correlations were not consistent with the data. As the intermediate state is either 2^+ or 2^-, the parent state must be either J^π=$3/2^\pm$ or $5/2^\pm$.

The angular correlations for the 14.1-MeV state in Fig. 17(a) are anisotropic and thus cannot be reproduced by pure $s_{1/2}$ and $p_{1/2}$ proton decay. The 3^+ intermediate state decays by ℓ=2 α emission. We have considered parent J^π states which decay by pure $p_{3/2}$ and $d_{5/2}$ proton emission. We have also considered mixed $p_{3/2}$ and $p_{1/2}$ and mixed $d_{5/2}$ and $s_{1/2}$ proton decays. The predicted angular correlations in the mixed decays depended on the relative amplitudes and phases of the two components. These were varied to best reproduce the data. The reduced χ^2 for parent J^π values which can reproduce the experimental correlations are listed in Table VI. The best fit for a positive ($3/2^+$ solid curve) and negative ($3/2^-$ dotted curve) parity assignments are shown in Fig. 17(a).

The experimental correlations for the state observed in the 2α+^{3}He channel are quite strong as shown in Fig. 18. Only with a parent of J^π=$7/2^+$ could we reproduce these data (χ^2/ν=0.97). The solid curve in the figure is obtained assuming an initial ℓ=1 decay for the first-step α emission. The second decay step must be ℓ=3 from spin and parity conservation. Given this high-spin state was observed in the 2α+^{3}He channel, one might question whether it is a member of a rotational band built on a configuration with strong α-cluster structure. A number of such bands have been observed, or proposed, in ^{11}C and its mirror ^{11}B [44, 45], but this state lies above all of these in energy.

VI. CONCLUSION

Application of the invariant-mass method is shown for a number of light isotopes using fast ^{13}O, ^{15}O, and ^{17}Ne beams. Proton pickup by these beam nuclei selectively populates d-wave resonances. The d-wave resonances observed in ^{16}F and ^{18}Na are consistent with previous studies. On the other hand, the invariant-mass spectrum obtained for ^{14}F is inconsistent with the previous work of Goldberg *et al.* [6]. We observe a prominent peak consistent with a 3^- state predicted by Sherr and Fortune [39]. This state may have been missed in [6] due to detector issues where a lower-energy peak was assigned as the 3^-

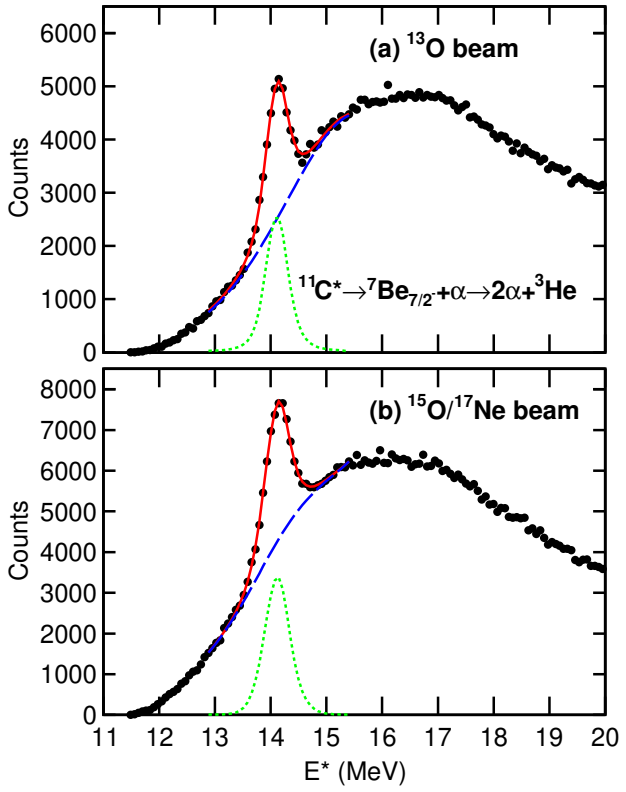

FIG. 16. Excitation-energy spectra for 2α+^{3}He events where there is a ^{7}Be($5/2^-$) intermediate state. Results shown were obtained with the (a) ^{13}O and (b) ^{15}O/^{17}Ne beams. Fits to these data (solid red curves) are shown where the fitted smooth backgrounds are given by the dashed blue curves.

state. We also find significant strength at lower energies indicating some d strength there as well. This is inconsistent with Ref. [6] which assigns only s-wave resonances in this region.

We have searched for the 4^+ member of a T=1 rotational band in ^{10}B which is the analog of bands built on the second 0^+ states in ^{10}Be and ^{10}C. A state near the expected energy was located in events that decay to ^{6}Li(T=1)+α, where the ^{6}Li(T=1) state γ decays to the ground state of ^{6}Li. By appropriately gating on detected γ-rays, a state in the ^{6}Li+α invariant-mass spectrum was isolated that was consistent with the J^π=4^+ member as suggested by Ref. [41]. Another example of using γ-ray gated was also shown in ^{16}F resonances.

A method of spin/parity determination has been investigated for states in ^{11}C that sequentially decay into three-body exit channels. From the distribution of angles between the two sequential decay axes, a peak at E^*=14.1 MeV in the invariant-mass spectrum of 2α+^{3}He events was assigned as J^π=$7/2^+$. Peaks in the ^{6}Li+α+p spectrum were also observed but here only restrictions to possible J^π values could be obtained.

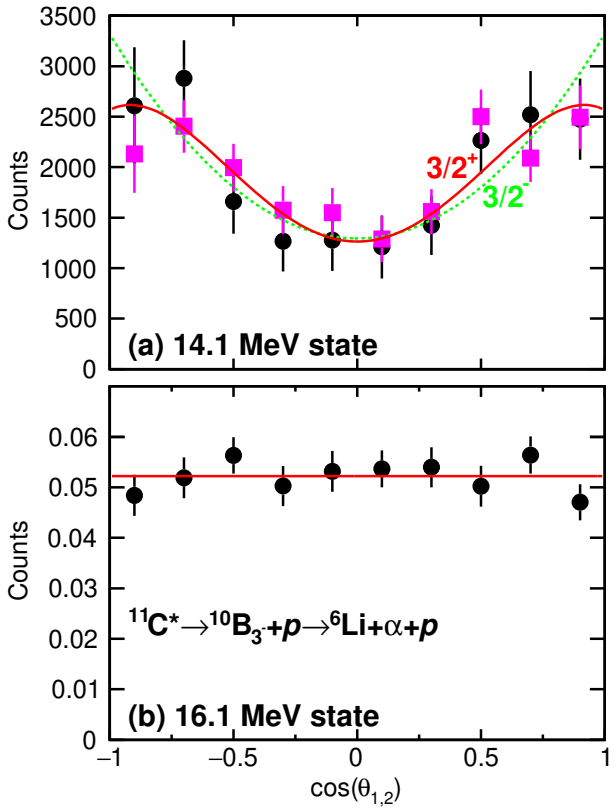

FIG. 17. Distributions of the angle between the two decay axes in the sequential decay for the (a) 14.1-MeV and (b) 16.1-MeV states observed in the ^{6}Li+α+p channel. Black circular data points were obtained for the ^{13}O data set while the square magenta ones are from the ^{15}O/^{17}Ne data set. The curves show examples of fits to these correlations. The solid and dashed curves in (a) show the best reproduction assuming the parent state has positive and negative parity, respectively, with the parent spins shown. In panel (b) the best reproduction is produced with a flat isotropic distribution (solid red curve).

ACKNOWLEDGMENTS

This material is based upon work supported by the U.S. Department of Energy, Office of Science, Office of Nuclear Physics under Award No. DE-FG02-87ER-40316.

[1] D. Brink, Kinematical effects in heavy-ion reactions, Phys. Lett. B **40**, 37 (1972).
[2] A. Gade, P. Adrich, D. Bazin, M. D. Bowen, B. A. Brown, C. M. Campbell, J. M. Cook, T. Glasmacher, K. Hosier, S. McDaniel, D. McGlinchery, A. Obertelli, L. A. Riley, K. Siwek, J. A. Tostevin, and D. Weisshaar, Inverse-

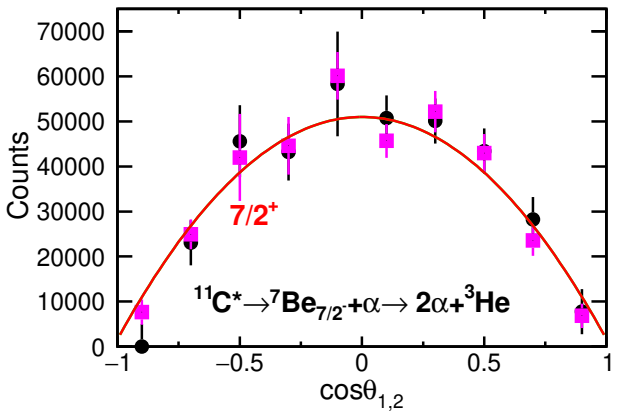

FIG. 18. Distributions of the angle between the two decay axes in the sequential decay of the 14.1-MeV state observed in the 2α+^{3}He channel. Circular black data points were obtained for the ^{13}O data set while the square magenta ones are from the ^{15}O/^{17}Ne data set. The curve shows the reproduction of the experimental correlation for a parent state of J^π=7/2$^+$.

TABLE VI. Spin-parity assignments consistent with the observed angular correlations θ_{12} obtained for the 14.1-MeV state in the ^{6}Li+α+p exit channel. Fits to the experimental correlations were obtained assuming an initial proton emission from the listed orbitals and the reduced χ^2 values are listed. For cases with contributions from multiple orbitals, the magnitude of each component and their relative phase was adjusted to give the best fit. For the two listed cases with multiple components, the best fit occurred when the two components are in phase and their relative contributions are given.

J^π	ℓ, j	χ^2/ν
3/2$^+$	$d_{5/2}$	0.70
5/2$^+$	72(21)% $d_{5/2}$, 28(21)% $s_{1/2}$	0.78
7/2$^+$	11(11)% $d_{5/2}$, 89(11)% $s_{1/2}$	1.13
11/2$^+$	$d_{5/2}$	1.17
3/2$^-$	$p_{3/2}$	1.21
9/2$^-$	$p_{3/2}$	1.44

kinematics one-proton pickup with intermediate-energy beams: The ^{9}Be (^{20}Ne,^{21}Na + γ)x reaction, Phys. Rev. C **76**, 061302(R) (2007).

[3] A. Gade, J. A. Tostevin, T. Baugher, D. Bazin, B. A. Brown, C. M. Campbell, T. Glasmacher, G. F. Grinyer, S. McDaniel, K. Meierbachtol, A. Ratkiewicz, S. R. Stroberg, K. A. Walsh, D. Weisshaar, and R. Winkler, Inverse-kinematics one-neutron pickup with fast rare-isotope beams, Phys. Rev. C **83**, 054324 (2011).

[4] A. Gade, J. A. Tostevin, V. Bader, T. Baugher, D. Bazin, J. S. Berryman, B. A. Brown, D. J. Hartley, E. Lunderberg, F. Recchia, S. R. Stroberg, Y. Utsuno, D. Weisshaar, and K. Wimmer, One-neutron pickup into ^{49}Ca: Bound neutron $g_{9/2}$ spectroscopic strength at N = 29, Phys. Rev. C **93**, 031601(R) (2016).

[5] R. J. Charity, K. W. Brown, J. Elson, W. Reviol, L. G. Sobotka, W. W. Buhro, Z. Chajecki, W. G. Lynch, J. Manfredi, R. Shane, R. H. Showalter, M. B. Tsang, D. Weisshaar, J. Winkelbauer, S. Bedoor, D. G. McNeel, and A. H. Wuosmaa, Invariant-mass spectroscopy of ^{18}Ne,^{16} O, and ^{10}C excited states formed in neutron-transfer reactions, Phys. Rev. C **99**, 044304 (2019).

[6] V. Goldberg, B. Roeder, G. Rogachev, G. Chubarian, E. Johnson, C. Fu, A. Alharbi, M. Avila, A. Banu, M. McCleskey, J. Mitchell, E. Simmons, G. Tabacaru, L. Trache, and R. Tribble, First observation of ^{14}F, Phys. Lett. B **692**, 307 (2010).

[7] M. Freer, E. Casarejos, L. Achouri, C. Angulo, N. I. Ashwood, N. Curtis, P. Demaret, C. Harlin, B. Laurent, M. Milin, N. A. Orr, D. Price, R. Raabe, N. Soić, and V. A. Ziman, $\alpha : 2n : \alpha$ molecular band in ^{10}Be, Phys. Rev. Lett. **96**, 042501 (2006).

[8] R. J. Charity, L. G. Sobotka, T. B. Webb, and K. W. Brown, Two-proton decay from α-cluster states in ^{10}C and ^{11}N, Phys. Rev. C **105**, 014314 (2022).

[9] Evaluated Nuclear Structure Data File (ENSDF), http://www.nndc.bnl.gov/ensdf/.

[10] M. Wallace, M. Famiano, M.-J. van Goethem, A. Rogers, W. Lynch, J. Clifford, F. Delaunay, J. Lee, S. Labostov, M. Mocko, L. Morris, A. Moroni, B. Nett, D. Oostdyk, R. Krishnasamy, M. Tsang, R. de Souza, S. Hudan, L. Sobotka, R. Charity, J. Elson, and G. Engel, The high resolution array (HiRA) for rare isotope beam experiments, Nucl Instrum. Methods A **583**, 302 (2007).

[11] K. W. Brown, R. J. Charity, L. G. Sobotka, Z. Chajecki, L. V. Grigorenko, I. A. Egorova, Y. L. Parfenova, M. V. Zhukov, S. Bedoor, W. W. Buhro, J. M. Elson, W. G. Lynch, J. Manfredi, D. G. McNeel, W. Reviol, R. Shane, R. H. Showalter, M. B. Tsang, J. R. Winkelbauer, and A. H. Wuosmaa, Observation of long-range three-body Coulomb effects in the decay of ^{16}Ne, Phys. Rev. Lett. **113**, 232501 (2014).

[12] K. W. Brown, R. J. Charity, L. G. Sobotka, L. V. Grigorenko, T. A. Golubkova, S. Bedoor, W. W. Buhro, Z. Chajecki, J. M. Elson, W. G. Lynch, J. Manfredi, D. G. McNeel, W. Reviol, R. Shane, R. H. Showalter, M. B. Tsang, J. R. Winkelbauer, and A. H. Wuosmaa, Interplay between sequential and prompt two-proton decay from the first excited state of ^{16}Ne, Phys. Rev. C **92**, 034329 (2015).

[13] K. W. Brown, R. J. Charity, J. M. Elson, W. Reviol, L. G. Sobotka, W. W. Buhro, Z. Chajecki, W. G. Lynch, J. Manfredi, R. Shane, R. H. Showalter, M. B. Tsang, D. Weisshaar, J. R. Winkelbauer, S. Bedoor, and A. H. Wuosmaa, Proton-decaying states in light nuclei and the first observation of ^{17}Na, Phys. Rev. C **95**, 044326 (2017).

[14] R. J. Charity, K. W. Brown, J. Okołowicz, M. Płoszajczak, J. M. Elson, W. Reviol, L. G. Sobotka, W. W. Buhro, Z. Chajecki, W. G. Lynch, J. Manfredi, R. Shane, R. H. Showalter, M. B. Tsang, D. Weisshaar, J. R. Winkelbauer, S. Bedoor, and A. H. Wuosmaa, Invariant-mass spectroscopy of ^{14}O excited states, Phys. Rev. C **100**, 064305 (2019).

[15] T. B. Webb, S. M. Wang, K. W. Brown, R. J. Charity, J. M. Elson, J. Barney, G. Cerizza, Z. Chajecki, J. Estee, D. E. M. Hoff, S. A. Kuvin, W. G. Lynch, J. Manfredi, D. McNeel, P. Morfouace, W. Nazarewicz, C. D. Pruitt,

C. Santamaria, J. Smith, L. G. Sobotka, S. Sweany, C. Y. Tsang, M. B. Tsang, A. H. Wuosmaa, Y. Zhang, and K. Zhu, First observation of unbound ^{11}O, the mirror of the halo nucleus ^{11}Li, Phys. Rev. Lett. **122**, 122501 (2019).

[16] T. B. Webb, R. J. Charity, J. M. Elson, D. E. M. Hoff, C. D. Pruitt, L. G. Sobotka, K. W. Brown, J. Barney, G. Cerizza, J. Estee, G. Jhang, W. G. Lynch, J. Manfredi, P. Morfouace, C. Santamaria, S. Sweany, M. B. Tsang, T. Tsang, S. M. Wang, Y. Zhang, K. Zhu, S. A. Kuvin, D. McNeel, J. Smith, A. H. Wuosmaa, and Z. Chajecki, Particle decays of levels in ^{11,12}N and ^{12}O investigated with the invariant-mass method, Phys. Rev. C **100**, 024306 (2019).

[17] T. B. Webb, R. J. Charity, J. M. Elson, D. E. M. Hoff, C. D. Pruitt, L. G. Sobotka, K. W. Brown, J. Barney, G. Cerizza, J. Estee, W. G. Lynch, J. Manfredi, P. Morfouace, C. Santamaria, S. Sweany, M. B. Tsang, T. Tsang, Y. Zhang, K. Zhu, S. A. Kuvin, D. McNeel, J. Smith, A. H. Wuosmaa, and Z. Chajecki, Invariant-mass spectrum of ^{11}O, Phys. Rev. C **101**, 044317 (2020).

[18] R. J. Charity, L. G. Sobotka, and J. A. Tostevin, Single-nucleon knockout cross sections for reactions producing resonance states at or beyond the drip line, Phys. Rev. C **102**, 044614 (2020).

[19] R. J. Charity, T. B. Webb, J. M. Elson, D. E. M. Hoff, C. D. Pruitt, L. G. Sobotka, K. W. Brown, G. Cerizza, J. Estee, W. G. Lynch, J. Manfredi, P. Morfouace, C. Santamaria, S. Sweany, C. Y. Tsang, M. B. Tsang, Y. Zhang, K. Zhu, S. A. Kuvin, D. McNeel, J. Smith, A. H. Wuosmaa, and Z. Chajecki, Observation of the exotic isotope ^{13}F located four neutrons beyond the proton drip line, Phys. Rev. Lett. **126**, 132501 (2021).

[20] D. Weisshaar, A. Gade, T. Glasmacher, G. F. Grinyer, D. Bazin, P. Adrich, T. Baugher, J. M. Cook, C. A. Diget, S. McDaniel, A. Ratkiewicz, K. P. Siwek, and K. A. Walsh, CAESAR-A high-efficiency CsI(Na) scintillator array for in-beam γ ray spectroscopy with fast rare-isotope beams, Nucl. Instrum. Methods A **624**, 615 (2010).

[21] A. M. Lane and R. G. Thomas, R-matrix theory of nuclear reactions, Rev. Mod. Phys. **30**, 257 (1958).

[22] I. Stefan, F. de Oliveira Santos, O. Sorlin, T. Davinson, M. Lewitowicz, G. Dumitru, J. C. Angélique, M. Angélique, E. Berthoumieux, C. Borcea, R. Borcea, A. Buta, J. M. Daugas, F. de Grancey, M. Fadil, S. Grévy, J. Kiener, A. Lefebvre-Schuhl, M. Lenhardt, J. Mrazek, F. Negoita, D. Pantelica, M. G. Pellegriti, L. Perrot, M. Ploszajczak, O. Roig, M. G. Saint Laurent, I. Ray, M. Stanoiu, C. Stodel, V. Tatischeff, and J. C. Thomas, Probing nuclear forces beyond the drip-line using the mirror nuclei ^{16}N and ^{16}F, Phys. Rev. C **90**, 014307 (2014).

[23] R. J. Charity, K. W. Brown, J. Okołowicz, M. Płoszajczak, J. M. Elson, W. Reviol, L. G. Sobotka, W. W. Buhro, Z. Chajecki, W. G. Lynch, J. Manfredi, R. Shane, R. H. Showalter, M. B. Tsang, D. Weisshaar, J. R. Winkelbauer, S. Bedoor, and A. H. Wuosmaa, Spin alignment following inelastic scattering of ^{17}Ne, lifetime of ^{16}F, and its constraint on the continuum coupling strength, Phys. Rev. C **97**, 054318 (2018).

[24] R. J. Charity and L. G. Sobotka, Invariant-mass spectroscopy in projectile-fragmentation reactions (2023), arXiv:2304.01124.

[25] W. Geithner, T. Neff, G. Audi, K. Blaum, P. Delahaye, H. Feldmeier, S. George, C. Guénaut, F. Herfurth, A. Herlert, S. Kappertz, M. Keim, A. Kellerbauer, H.-J. Kluge, M. Kowalska, P. Lievens, D. Lunney, K. Marinova, R. Neugart, L. Schweikhard, S. Wilbert, and C. Yazidjian, Masses and charge radii of $^{17-22}$Ne and the two-proton-halo candidate ^{17}Ne, Phys. Rev. Lett. **101**, 252502 (2008).

[26] C. Lehr, F. Wamers, F. Aksouh, Y. Aksyutina, H. Ávarez Pol, L. Atar, T. Aumann, S. Beceiro-Novo, C. Bertulani, K. Boretzky, M. Borge, C. Caesar, M. Chartier, A. Chatillon, L. Chulkov, D. Cortina-Gil, P. Diáz Fernández, H. Emling, O. Ershova, L. Fraile, H. Fynbo, D. Galaviz, H. Geissel, M. Heil, M. Heine, D. Hoffmann, M. Holl, H. Johansson, B. Jonson, C. Karagiannis, O. Kiselev, J. Kratz, R. Kulessa, N. Kurz, C. Langer, M. Lantz, T. Le Bleis, R. Lemmon, Y. Litvinov, B. Löher, K. Mahata, J. Marganiec-Galązka, C. Müntz, T. Nilsson, C. Nociforo, W. Ott, V. Panin, S. Paschalis, A. Perea, R. Plag, R. Reifarth, A. Richter, K. Riisager, C. Rodriguez-Tajes, D. Rossi, D. Savran, H. Scheit, G. Schrieder, P. Schrock, H. Simon, J. Stroth, K. Sümmerer, O. Tengblad, H. Weick, and C. Wimmer, Unveiling the two-proton halo character of ^{17}Ne: Exclusive measurement of quasi-free proton-knockout reactions, Phys. Lett. B **827**, 136957 (2022).

[27] M. Wang, W. J. Huang, F. G. Kondev, G. Audi, and S. Naimi, The ame 2020 atomic mass evaluation (ii). tables, graphs and references, Chin. Phys. C **45**, 030003 (2021).

[28] T. Baugher, *Neutron-rich chromium and manganese isotopes and the role of the neutron $0g_{9/2}$ and $1d_{5/2}$ orbitals in the region below ^{68}Ni*, Ph.D. thesis, Michigan State University (2013).

[29] V. Bader, *Quadrupole collectivity in neutron-deficient Sn nuclei: ^{104}Sn*, Ph.D. thesis, Michgan State University (2014).

[30] B. A. Brown, A. Etchegoyen, and W. D. M. Rae, *The computer code OXBASH*, Tech. Rep. MSU-NSCL 524 (NSCL Michigan State University, Michigan, 1994).

[31] E. K. Warburton and B. A. Brown, Effective interactions for the 0p1s0d nuclear shell-model space, Phys. Rev. C **46**, 923 (1992).

[32] T. Zerguerras, B. Blank, Y. Blumenfeld, T. Suomijärvi, D. Beaumel, B. Brown, M. Chartier, M. Fallot, J. Giovinazzo, C. Jouanne, V. Lapoux, I. Lhenry-Yvon, W. Mittig, P. Roussel-Chomaz, H. Savajols, J. Scarpaci, A. Shrivastava, and M. Thoennessen, Study of light proton-rich nuclei by complete kinematics measurements, Eur. J. Phys. A **20**, 389 (2004).

[33] M. Assié, F. de Oliveira Santos, T. Davinson, F. de Grancey, L. Achouri, J. Alcántara-Núñez, T. Al Kalanee, J.-C. Angélique, C. Borcea, R. Borcea, L. Caceres, I. Celikovic, V. Chudoba, D. Pang, C. Ducoin, M. Fallot, O. Kamalou, J. Kiener, Y. Lam, A. Lefebvre-Schuhl, G. Lotay, J. Mrazek, L. Perrot, A. Sánchez-Benítez, F. Rotaru, M.-G. Saint-Laurent, Y. Sobolev, N. Smirnova, M. Stanoiu, I. Stefan, K. Subotic, P. Ujic, R. Wolski, and P. Woods, Spectroscopy of ^{18}Na: Bridging the two-proton radioactivity of ^{19}Mg, Phys. Lett. B **712**, 198 (2012).

[34] I. Mukha, L. Grigorenko, L. Acosta, M. A. G. Alvarez, E. Casarejos, A. Chatillon, D. Cortina-Gil, J. M. Espino, A. Fomichev, J. E. García-Ramos, H. Geissel, J. Gómez-

Camacho, J. Hofmann, O. Kiselev, A. Korsheninnikov, N. Kurz, Y. A. Litvinov, I. Martel, C. Nociforo, W. Ott, M. Pfützner, C. Rodríguez-Tajes, E. Roeckl, C. Scheidenberger, M. Stanoiu, K. Sümmerer, H. Weick, and P. J. Woods, New states in ^{18}Na and ^{19}Mg observed in the two-proton decay of ^{19}Mg, Phys. Rev. C **85**, 044325 (2012).

[35] G. Zeeb, M. Reiter, and M. Bleicher, Multi-strange baryon production in Au+Au collisions near threshold, Phys. Lett. B **586**, 297 (2004).

[36] N. Aoi, K. Yoneda, E. Ideguchi, T. Kishida, T. Nakamura, M. Notani, H. Sakurai, T. Teranishi, Y. Watanabe, H. Wu, A. Yoshida, H. Miyatake, Y. Yamamoto, H. Ogawa, S. S. Yamamoto, and M. Ishihara, Anomaly of $N = 8$ shell closure in neutron-rich Be and B isotopes studied via delayed neutron emitting ^{14}Be β decay, Phys. Rev. C **66**, 014301 (2002).

[37] H. Fortune, Population of bound and unbound states of ^{12}Be in proton removal from ^{13}B, Phys. Lett. B **755**, 351 (2016).

[38] A. Krieger, K. Blaum, M. L. Bissell, N. Frömmgen, C. Geppert, M. Hammen, K. Kreim, M. Kowalska, J. Krämer, T. Neff, R. Neugart, G. Neyens, W. Nörtershäuser, C. Novotny, R. Sánchez, and D. T. Yordanov, Nuclear charge radius of ^{12}Be, Phys. Rev. Lett. **108**, 142501 (2012).

[39] R. Sherr and H. Fortune, Low-lying resonances in ^{14}F and ^{14}B, Phys. Lett. B **699**, 281 (2011).

[40] A. N. Kuchera, G. V. Rogachev, V. Z. Goldberg, E. D. Johnson, S. Cherubini, M. Gulino, M. La Cognata, L. Lamia, S. Romano, L. E. Miller, R. G. Pizzone, G. G. Rapisarda, M. L. Sergi, C. Spitaleri, R. E. Tribble, W. H. Trzaska, and A. Tumino, Molecular structures in $T = 1$ states of ^{10}B, Phys. Rev. C **84**, 054615 (2011).

[41] O. S. Kirsebom, M. Alcorta, M. J. G. Borge, M. Cubero, H. O. U. Fynbo, M. Madurga, and O. Tengblad, Observation of α decay from a state in ^{10}B at 11.48 MeV, Phys. Rev. C **85**, 054308 (2012).

[42] L. C. Biedenharn and M. E. Rose, Theory of angular correlation of nuclear radiations, Rev. Mod. Phys. **25**, 729 (1953).

[43] H. Frauenfelder, Angular correlation of nuclear radiation, Annu. Rev. Nucl. Sci. **2**, 129 (1953).

[44] N. Soić, M. Freer, L. Donadille, N. Clarke, P. Leask, W. Catford, K. Jones, D. Mahboub, B. Fulton, B. Greenhalgh, D. Watson, and D. Weisser, α-decay of excited states in 11c and 11b, Nucl. Phys. A **742**, 271 (2004).

[45] H. Yamaguchi, T. Hashimoto, S. Hayakawa, D. N. Binh, D. Kahl, S. Kubono, Y. Wakabayashi, T. Kawabata, and T. Teranishi, α resonance structure in ^{11}B studied via resonant scattering of ^{7}Li+α, Phys. Rev. C **83**, 034306 (2011).